A Reliable CMOS-MEMS Platform for Titanium Nitride Composite (TiN-C) Resonant Transducers with Enhanced Electrostatic Transduction and Frequency Stability

Ming-Huang Li, Chao-Yu Chen, and Sheng-Shian Li

Institute of NanoEngineering and MicroSystems, National Tsing Hua University, Hsinchu 30013, Taiwan
Phone: +886-3-571-5131 ext.80631, Fax: +886-3-574-5454, Email: s100035807@m100.nthu.edu.tw

Abstract

A reliable CMOS-MEMS platform for on-chip resonant transducer and readout circuit integration is presented in this paper with (i) well-defined etch stops and relaxed release windows for high fabrication yield, (ii) narrow transducer gaps (< 400nm) for efficient electrostatic transduction, and (iii) novel titanium nitride composite (TiN-C) structure for dielectric charge elimination and temperature compensation. With the proposed platform, MEMS resonant transducers which exhibit low frequency drift over temperature and time, excellent electrostatic coupling, and inherent CMOS circuit integration are successfully demonstrated.

I. Introduction

Over the past few years, the strong demands on emerging internet of things (IoT) and wearable devices become a major driven force for developing smart sensor systems toward the smart life. Due to the benefit from mass production capability and inherent circuit integration, the commercially-available CMOS-MEMS platforms [1]-[5] offer a cost-effective solution to allow the realization of a compact sensor system, including timing reference, signal processing and multi-sensors building blocks. Table I summarizes the performance comparison among state-of-the-art CMOS-MEMS technologies.

However, the weak electrostatic coupling still plays a major obstacle on the practical applications, especially for capacitive resonant transducers. To address this issue, a narrow gap feature is widely used to reduce the motional impedance (R_m). With the two-polysilicon configuration in a standard 0.35μm process, it is able to achieve the tiny transduction gap of only 40nm [1] for lateral vibration but at the cost of limited transduction area and probably lower yield. On the other hand, the polysilicon release process [2] was reported recently to create an oxide-rich high-Q resonator with exact 180nm air-gap. However, these techniques are difficult to extend to advanced technology nodes due to the restriction of FEOL layers (i.e., single-polysilicon processes).

Although the oxide-rich design is preferred to attain the high-Q response based on our previous work [2][5], the CMOS-MEMS resonant transducer often faces the frequency drift issue over long elapsed time due to the undesired inter-gap dielectric charging phenomenon [3]. In this work, we attempt to develop a novel titanium nitride composite (TiN-C) structure existing in Al-based BEOL that can achieve not only the decent transducer gap for efficient transduction, but also the excellent frequency stability as compared to CMOS-MEMS resonator work to date.

II. TIN-C Resonator

As a design example, Fig. 1(a) shows the simplified layout and cross-sectional view of the proposed TiN-C "pseudo" free-free beam (PFFB) CMOS-MEMS resonator in a four-terminal (4T) configuration. To realize a multiple-port TiN-C resonator, the *oxide fins* are used to separate two TiN conductive films from each other for electrical isolation. For maximizing the Q-factor, the oxide fins are placed at the corresponding vibrating nodal points of the free-free beam mode shape [6]. Fig. 1(b) shows the resonator dimension and simulated mode shape. In this design, the silicon substrate (i.e., the "Body" terminal) should be properly *grounded* to suppress the undesired electrical feedthrough signal.

The fabrication process for the titanium nitride composite (TiN-C) structure is depicted in Fig. 2. The CMOS chip before post-processing is shown in Fig. 2(a) where the composite sacrificial metal layer is exposed and electrical routings are protected by the top metal capping layers. Then, the composite sacrificial layer is removed by sulfuric acid (H_2SO_4) with hydrogen peroxide (H_2O_2) at around 100°C, as illustrated in Fig. 2(b). After the metal wet etching process, the exposed oxide layer and TiN layer are then removed by a two-step reactive ion etching process (Fig. 2(c)). Next, the exposed AlCu core metal is etched by a commercial Al-etchant with a very high selectivity with TiN, oxide, and tungsten (W) vias (Fig. 2(d)). This step also removes the protective top metal (i.e., M4 capping layer). After this step, the MEMS resonator is free to vibrate. For later device testing, the two-step RIE is again used to expose the probing pads, as depicted in Fig. 2(e).

Since we have allocated proper etch-stops in every process steps, the undercut can be precisely controlled to keep compact footprint. Thus a robust and *high process yield of > 90%* (more than 10 chips were released and tested) is achieved with the post-CMOS process in an academic cleanroom.

The optical views for the fabricated devices are shown in Fig. 3 and the optical interferometer is used to evaluate the radius of curvature (R.O.C) of the resonators (cf. Fig. 4). The PFFB resonator is very flat (R.O.C. > 24.9mm) after release, while the cantilever beam curves up (R.O.C. > 1.61mm) due to its bimorph feature. Moreover, the SEM pictures are shown in Fig. 5, indicating a tiny gap of 400nm for efficient electrostatic transduction.

III. Experimental Results

A. Frequency Characteristics

In this work, various resonator designs are applied to verify the performance of this platform, and the measurement results are summarized in Table II where the resonator frequency ranges from 2.7 MHz to 14.2 MHz, and the tested bias voltage (V_P) ranges from 5V to 85V. Fig. 6(a) illustrates the test setup of the two-port measurement for a 4T CMOS-MEMS resonator without using any amplification circuit, where the body terminal is connected to ground. As shown in Fig. 6(b), the background feedthrough is effectively suppressed by 17 dB at 15 MHz. With the body-grounded technique, the resonance spectrum exhibits a 15-dB stopband rejection. The 11.5-MHz PFFB resonator features Q of 1,400 and motional impedance (R_m) of 390 kΩ under V_P of 70 V. Fig. 7 further presents the measured spectra of two kinds of clamped-clamped beam (CCB) resonators under a 1-port configuration. A medium-V_P of 35 V is sufficient to achieve a low-R_m of 35 kΩ for a 2.7-MHz CCB resonator.

B. Frequency Stability

The frequency stability for CMOS-MEMS resonators is a vital issue for emerging applications. The dielectric charging phenomenon [3] placed a bottleneck for conventional (i.e., oxide-metal) CMOS-MEMS resonators [2][3][5] because of unpredictable frequency drifting with elapsed time. In this work, the TiN-C MEMS resonators effectively solve this problem since there is no dielectric between the electrostatic transducer gaps. To verify, a *reverse-biasing* scheme [7] is used to investigate the charging issue. As shown in Fig. 8, perfectly overlapped resonance spectra for the TiN-C resonator are confirmed for both +70 V and -70 V bias. It indicates that the dielectric charging is not observed for the TiN-C resonator. However, for a conventional CMOS-MEMS resonator in [5], the frequency spectra for +/-70V bias are separated, revealing severe dielectric charging effects [7]. Moreover, the resonance frequency for both oxide-metal (device from [5]) and TiN-C resonator (this work) are continuously tracked for the first 40 minutes under an elevated temperature as V_P is applied (cf. Fig. 9). Similar to the case in [3] and [7], the resonator with the inter-gap dielectric shows a tremendous frequency drift (> 2,500 ppm) caused by dielectric charging. In contrast, there is *no apparent frequency drift observed for the TiN-C resonator*.

As a result, the proposed TiN-C resonator fundamentally solves the dielectric charging problem while enhancing the electrostatic coupling with its 400nm tiny-gap. The frequency stability against temperature variation is also tested among three different resonator designs. The lowest temperature coefficient of frequency (TC_f) of only *0.6 ppm/K* is measured for an 11.5-MHz PFFB resonator (cf. Fig. 10). This is an unprecedented TC_f (sub-ppm/K) in CMOS-MEMS resonators with only a *passive* temperature compensation scheme. Table III further summarizes the TC_f's for different resonators. Although the same BEOL stacking is used, there is a clear difference on the 1st TC_f between the first and second mode PFFB. The possible reason is that the device's TC_f is now highly related to the axial mechanical stress from oxide fins.

C. Circuit Integration and Outlook

Fig. 11 finally presents the frequency spectra for the monolithically-integrated MEMS resonator circuit, showing a 40-dB enhancement compared to a standalone version. With an integrated amplifier, the motional signal can be detected even with a low-V_P of 5 V (equivalent R_m > 289MΩ). In the future, the potential of this platform will be maximized with array designs and advanced technology nodes (cf. Fig. 12, Fig. 13). If a multi-resonator array is designed, the required V_P will be dramatically reduced, which also benefits the resonator linearity. In addition, the advanced technology would provide more BEOL (back-end of line) layers for routing and MEMS design flexibility.

IV. Conclusions

In this work, we have successfully demonstrated the innovative titanium nitride composite (TiN-C) structure with high post-process yield in a foundry-oriented CMOS-MEMS platform. The proposed TiN-C resonator shows the lowest TC_f of 0.6 ppm/K in CMOS-MEMS technology to date with a well-defined transduction gap of 400nm. The proposed TiN-to-TiN gap provides an attractive feature to eliminate the charge-induced frequency drift in a standard CMOS-MEMS platform, revealing the excellent frequency stability over temperature and time for practical applications in the future.

Acknowledgements. This research was sponsored by the MOST of Taiwan (MOST-103-2221-E-007-113-MY3). The chip fabrication is supported by CIC and TSMC, Taiwan.

Reference

[1] J. Lopez *et al.*, *IEEE Electron Device Lett.*, vol. 30, no. 7, pp. 718-720, 2009.

[2] C.-H. Chin *et al.*, *J. Micromech. Microeng.*, vol.24, no.9, pp. 095005, 2014.

[3] K. Dorsey and G. Fedder, *Proc. IEEE Sensors'10*, pp. 197-200, 2010.

[4] A. Uranga *et al.*, *Proc. IEEE MEMS'15*, pp. 1004-1007, 2015.

[5] M.-H. Li *et al.*, *J. Microelectromech. Syst.*, vol. 24, no. 2, pp. 360-372, Apr. 2015.

[6] K. Wang *et al.*, *J. Microelectromech. Syst.*, vol. 9, no. 3, pp. 347-360, Sep. 2000.

[7] G. Bahl *et al.*, *J. Microelectromech. Syst.*, vol. 19, no. 1, pp. 162-174, Feb. 2010.

Table I: Comparison of CMOS-MEMS platforms for resonant transducers.

Reference	[1]	[2]	[3]	[4]**	[5]	This Work
CMOS Technology (Standard/ Modified)	Standard, 350 nm	Standard, 350 nm	Standard, 350 nm	Modified, 180nm	Standard, 350 nm	Standard, 350 nm
Tech. Scalability	Yes	Yes	No*	Yes	Yes	Yes***
Gap Sacrificial Layer	AlCu + W	Poly-Si	Oxide	Polymer	Oxide	AlCu
Effective Capacitive Transducer Gap	1μm	300nm	40nm	100nm	1μm	400nm
Capacitive Transduction Area	Medium	Large	Small	Small	Medium	Large
Resonator Type	Lateral Tuning Fork	Vertical CC-Beam	Lateral Beam	Torsional Bar	Lateral Cantilever	Vertical Beam
Resonator Material	Metal + IMD	Metal + IMD	Poly-Si	Bi-Metallic Nitride	Metal + IMD	Metal + IMD
Dielectric Charging	Yes	Yes	No	No	Yes	No
†Best- Case TCF [ppm/K]	5.1 (Passive) < 1 (Ovenized)	-	-	-	-	0.6 (Passive)

† Temperature coefficient of frequency. * Limited to 2-poly CMOS process for 40-nm gap define.
** MEMS resonator is formed by a post-CMOS deposited bi-metallic nitride.
*** Can be scaled to other AlCu-BEOL CMOS process, e.g., 250 nm/ 180 nm.

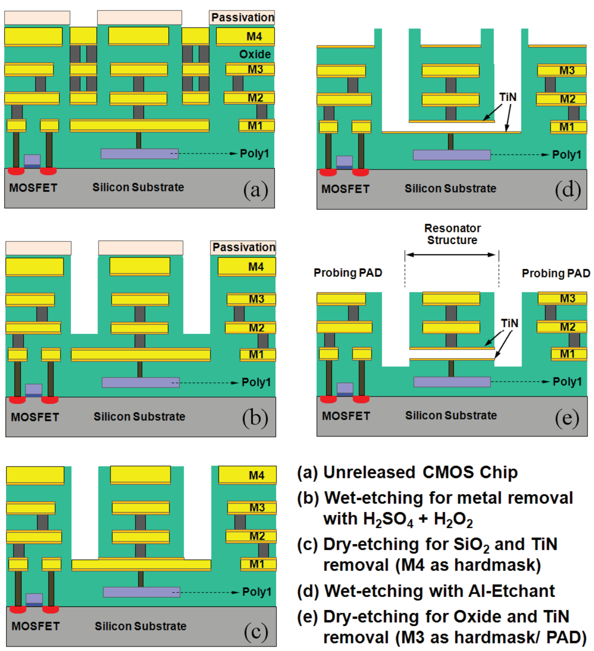

Fig. 2: Proposed maskless post-CMOS process for TiN-C CMOS-MEMS resonators. A 350-nm 2P4M standard CMOS process is used in this work.

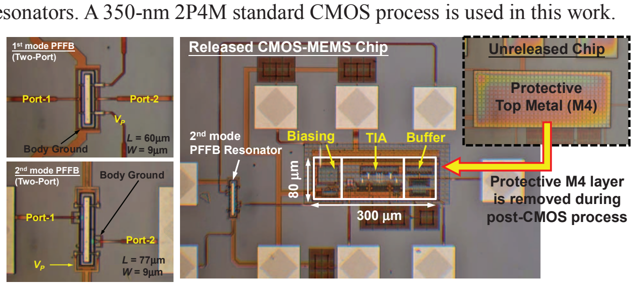

Fig. 3: Optical photos of the MEMS resonators and MEMS + CMOS circuit.

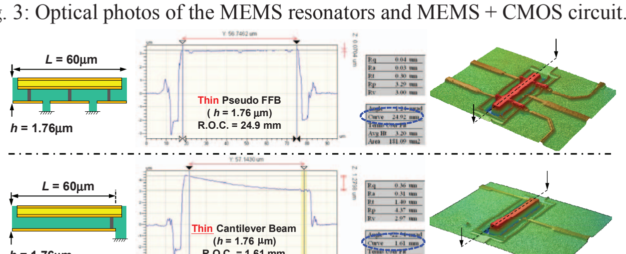

Fig. 4: Measured radius of curvature (R.O.C.) and surface profile of selected resonator test keys using optical interferometer. The worst-case R.O.C. of 1.61 mm is obtained with a bimorph-like cantilever beam (M2 + IMD + TiN).

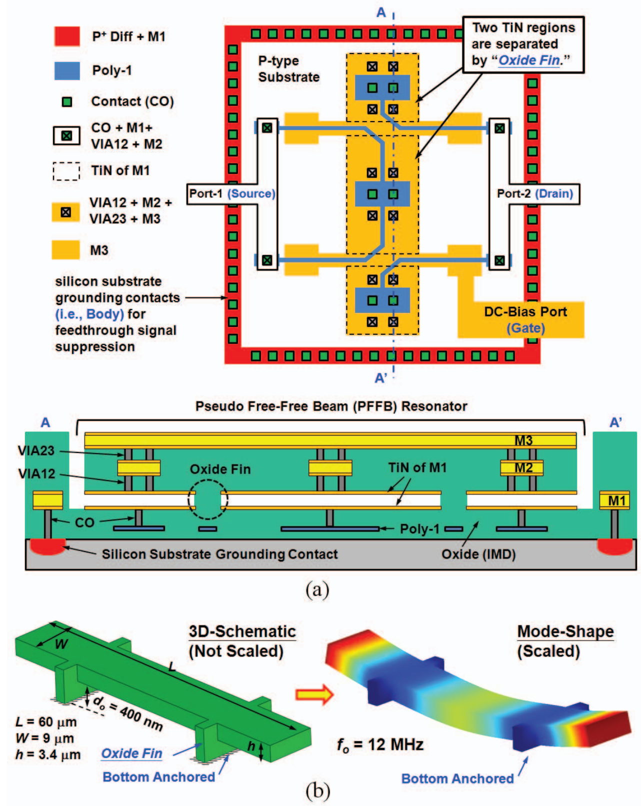

Fig. 1: (a) Layout and cross-sectional views of a TiN-C two-port 1st-mode "pseudo" free-free beam (PFFB) resonator as a design example. (b) Schematic and mode-shape of the 1st-mode PFFB resonator.

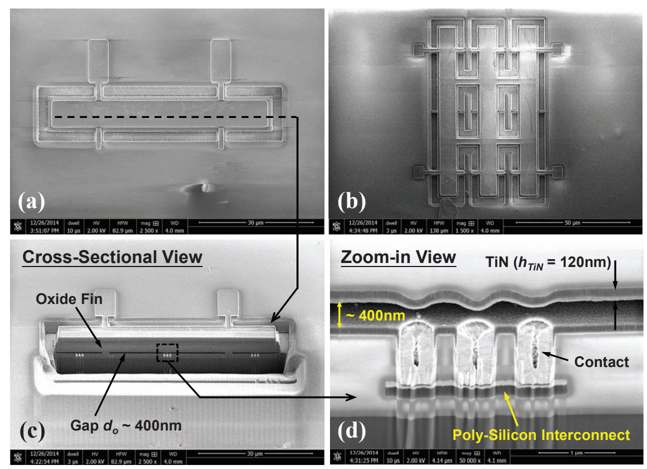

Fig. 5: SEM views of the CMOS-MEMS resonators. (a) Top view of the 1st-mode PFFB. (b) Top view of the 2nd-mode PFFB array. (c) Cross-sectional view of the PFFB. (d) Zoom-in view of the 400-nm gap.

Table II: Summary of characterized TiN-C MEMS resonators.

Device	CC-Beam	CC-Beam	1st mode PFFB	1st mode PFFB	2nd mode PFFB
Configuration	1-Port	1-Port	2-Port	2-Port	2-Port
Length (μm)	60	60	60	60	77
Thickness (μm)	1.76	3.4	1.76	3.4	3.4
Frequency (MHz)	2.7	4.7	8.2	11.5	14.2
DC-Bias for Device Testing	20 - 35	20 - 50	35 - 70	35 - 70	5 - 85
Q-factor in Vacuum (Q-factor in Air)	1000	1471	1832	1410 (330)	630 (260)
Measured R_m (kΩ)	70 (V_P = 35V)	100 (V_P = 50V)	178 (V_P = 70V)	335 (V_P = 70V)	1000 (V_P = 85V)

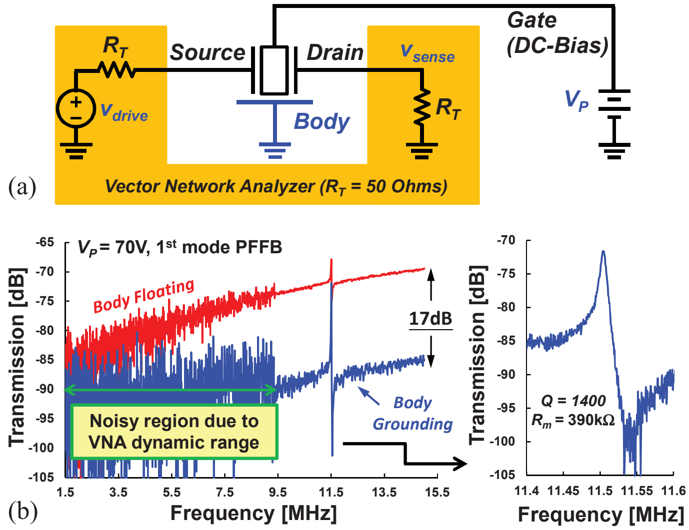

Fig. 6: Measurement schemes. (a) Typical measurement setup for a 4-terminal (4T) TiN-C CMOS-MEMS resonator. (b) Demonstration of feedthrough suppression by 17 dB at 15 MHz using body grounding scheme (measured without circuits).

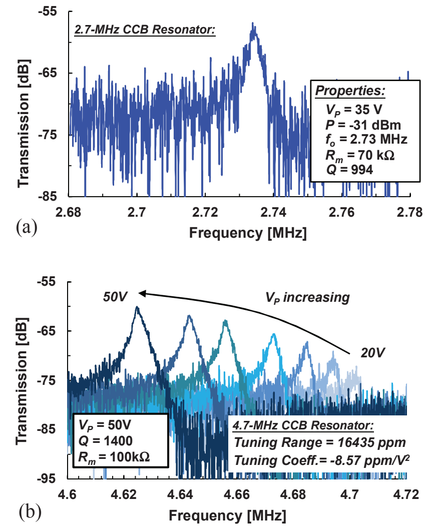

Fig. 7: Open loop testing of the TiN-C resonators (measured without circuits). (a) A 2.7-MHz CCB resonator with low R_m of 70 kΩ. (b) Frequency tuning of a 4.7-MHz CCB resonator.

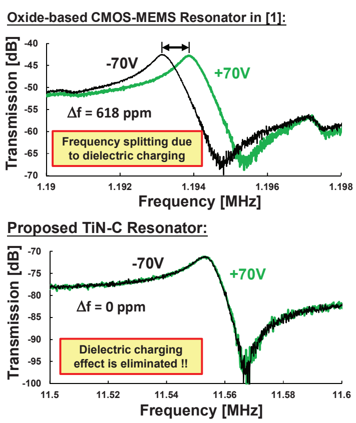

Fig. 8: *Reverse-biasing* test [7] for demonstration of the dielectric charge elimination scheme in TiN-C resonators. The frequency spilt of 618 ppm is observed in a CMOS-MEMS oxide resonator [1].

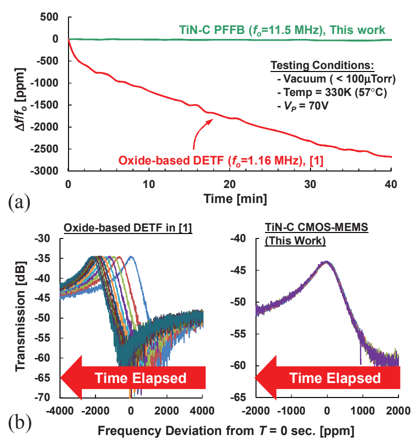

Fig. 9: (a) Measured short-term frequency drift over time for the first 40 minutes under an elevated chamber temperature of 330 K. (b) Selected transmission curves of the tested resonators within the first 30 minutes as V_P = 70V is engaged.

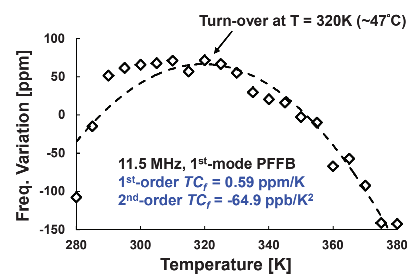

Fig. 10: Measured temperature coefficient of frequency (TC_f) of an 11.5-MHz, temperature-compensated 1st mode pseudo free-free beam resonator.

Table III: Summary of measured TC_f's.

Device	1st mode PFFB	1st mode PFFB	2nd mode PFFB
Frequency [MHz] (T = 293 K)	8.205	11.507	14.193
Thickness (μm)	1.76	3.4	3.4
1st TC_f (ppm/K)	-132	0.59	-30
2nd TC_f (ppb/K²)	-174	-64.9	-8.4

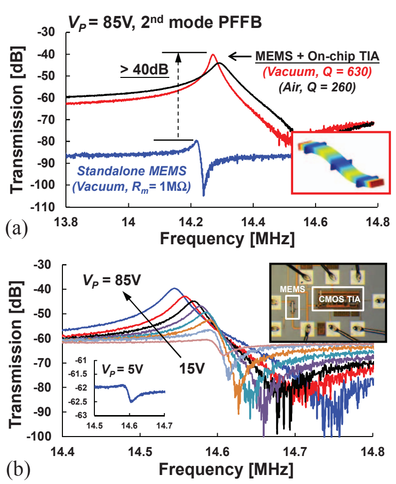

Fig. 11: Measurement of the 2nd mode PFFB resonator with *integrated* CMOS readout circuit. (a Transmission comparison. (b) Biasing voltage frequency/transmission tuning.

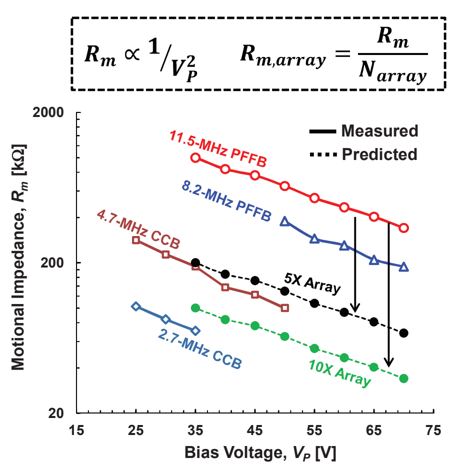

Fig. 12: Measured and predicted R_m for the TiN-composite CMOS-MEMS resonators. With array technique, an R_m of 100 kΩ for 11.5-MHz PFFB resonator can be achieved by a medium-V_P of only 35V.

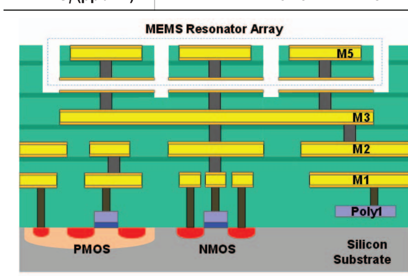

Technology	CMOS Routing	Sacrificial Layer	MEMS
350 nm, 2P4M	P1, P2, M1–M3	Mn, n = 1–2	M2 – M3
180 nm, 1P6M	P1, M1–M5	Mn, n = 1–4	M2 – M5
180 nm, 1P6M [MEMS-above-CMOS]	P1, M1–M3	M4	M5

Fig. 13: Future implementation in 180-nm node for MEMS-above-CMOS designs. The table provides possible design options (assume at least 3-metal layers are required for CMOS circuit routings).